JOURNAL OF THERMOPHYSICS AND HEAT TRANSFER
Vol. 11, No. 4, October–December 1997

Assessment of Thermochemical Nonequilibrium and Slip Effects for Orbital Re-Entry Experiment

Roop N. Gupta,* James N. Moss,† and Joseph M. Price‡
NASA Langley Research Center, Hampton, Virginia 23681-0001

Results are provided from a viscous shock layer (VSL) analysis of the re-entry flowfield around the forebody of the Japanese Orbital Re-entry Experiment (OREX) vehicle. This vehicle is a 50-deg spherically blunted cone with a nose radius of 1.35 m and a base diameter of 3.4 m. Calculations are performed for the OREX trajectory from a 105 to 48.4 km altitude range. A seven-species chemical model for air is found adequate for the flowfield analysis. However, for altitudes greater than 84 km, the low-density effects (such as thermal nonequilibrium and slip) must be implemented to accurately predict flight-inferred heat transfer rate data. At altitudes lower than 84 km, a finite surface recombination probability employed in place of a noncatalytic surface enhances the agreement between the calculations and flight data. VSL results are also compared with the direct simulation Monte Carlo predictions at high altitudes (>80 km) and the electron number density data for three altitudes in the OREX trajectory. Overall, the agreement between the flight data and calculated results is quite good.

Nomenclature

d	=	base diameter, m
Kn_∞	=	freestream Knudsen number, λ_∞/d
L	=	shuttle length, m
M_∞	=	freestream Mach number
p_w	=	surface pressure, N/m^2
q_w	=	surface heating rate, W/m^2
R_N	=	nose radius, m
s	=	distance along the body surface measured from the stagnation point, m
T_{ve}	=	vibrational–electronic–electron excitation temperature, K
T_w	=	surface temperature, K
T_∞	=	freestream temperature, K
V_∞	=	freestream velocity, m/s
X_i	=	mole fraction of species i
x	=	axial distance from stagnation point measured along symmetry axis, m
y	=	radial distance from symmetry axis, m
γ_O, γ_N	=	recombination probabilities for atomic oxygen and nitrogen, respectively
η_e	=	electron number density, m^{-3}
λ_∞	=	mean free path, m
ρ_∞	=	freestream density, kg/m^3

Introduction

FOR the optimum design of reusable space transportation vehicles, it is necessary to determine the re-entry aerothermal environment of these vehicles accurately so that the weight of the thermal protection system may be minimized to increase the payload capacity. An accurate prediction by computational fluid dynamics (CFD) methods of surface heating, temperature, and flowfield quantities during re-entry naturally requires accurate modeling of the flowfield chemistry, gas–surface interaction, body (and shock) slip, as well as the thermochemical nature of the flowfield.[1] Because of the extreme physical conditions encountered and associated modeling difficulties, it becomes essential to calibrate the CFD codes, ideally against flight data, for a wide range of flow conditions. Some of the codes show good accuracies against ground-test results, which, in general, do not simulate high-temperature real-gas effects as encountered in a hypervelocity flight. Thus, the code comparison against the flight data cannot be overemphasized, especially, for high energy flows. The Orbital Re-entry Experiment (OREX) was conducted recently from orbit to create a database to study the re-entry technology, and to establish the accuracy of computational design tools for Earth-Space Round Trip (ESRT) systems.[2]

OREX was the first of the three flight experiments planned to obtain the technology base for the development of Japan's unmanned space shuttle called HOPE (H-II Orbiting Plane). OREX was launched into Earth orbit by the H-II rocket on Feb. 4, 1994, and was the first Japanese entry experiment. Two of the many OREX objectives were to 1) gather re-entry data (such as those for the aerodynamic performance and aerothermal environment and guidance/navigation/control), and 2) test the thermal protection system that has been developed for HOPE. For meeting the second objective, the maximum heating rate encountered by OREX was almost equal to that computed for HOPE (Ref. 2). The initial reports provide an indication of the scope and quality of the basic data acquired.[2,3]

The inferred surface heating rate data for OREX are considered potentially unique for altitudes above about 92 km. Unlike the Shuttle Orbiter, which is an operational vehicle, OREX was enclosed in a protective fairing during launch, thereby negating the requirement for waterproofing the thermal protection materials. Consequently, the OREX thermal protection system did not produce some of the outgassing products and the associated reduction in heating measured for the Orbiter during the initial phase of the heat pulse.[4] A motivation, therefore, exists for the comparison of numerical predictions with the OREX data. Reference 3 presents a seven-species, one-temperature (1-T) analysis of the OREX stagnation-point heating data. The computations of Ref. 3 were recently redone with new values for the thermal properties of the carbon/carbon (C/C) nose cap.[5] The low-density effects (such as the thermochemical nonequilibrium and slip) were not considered in

Received July 29, 1996; revision received April 3, 1997; accepted for publication April 4, 1997.

*Senior Research Engineer, Aero & Gas Dynamics Division. Associate Fellow AIAA.

†Senior Research Engineer, Aero & Gas Dynamics Division. Fellow AIAA.

‡Senior Research Engineer, Aero & Gas Dynamics Division.

the analyses of Refs. 3 and 5. In the data reduction procedure for the electrostatic probe,[2] however, a two-temperature (2-T) calculation method was employed without the surface-slip effects.[6]

In the present study, the OREX aerothermodynamic data are analyzed by using the viscous shock layer (VSL) technique of Ref. 1. This technique is used to calculate flowfield and surface quantities along the OREX forebody for altitudes of 105–48.4 km. Information concerning the surface temperature was obtained from Yamamoto[5] for these altitudes. Comparisons of VSL results with flight data include stagnation-point heating rates and the flowfield electron number densities. An assessment of the low-density effects (such as thermochemical nonequilibrium and slip) on surface heating and flowfield quantities is made by comparison with the direct simulation Monte Carlo (DSMC) results obtained from the method of Bird[7] and the flight data.

Problem Definition and Methodology

OREX Geometry and Sensor Locations

The OREX vehicle is a 50-deg spherically blunted cone with a 1.35-m nose radius and a base diameter of 3.4 m (Fig. 1). It was launched into Earth orbit using Japan's new H-II launch vehicle. During entry, aerothermal data were obtained from altitudes of about 120 km down to about 40 km, including the blackout period when the maximum heating occurred.

The measurements for which the data are compared with current VSL and DSMC calculations are 1) the inferred heating rates extracted (Ref. 8) from the back surface (with material thickness of 4 mm) temperature measurements made at the nose cap stagnation point, and 2) the electron number density distribution in the boundary layer measured by an electrostatic probe mounted on the conical flank before the probe shoulder. The electrostatic probe protrudes from the OREX vehicle surface 70 mm in height. Five semicylindrical electrodes of 0.2 mm diam are situated along the leading edge of the probe with 0.4 mm bluntness and 60-deg sweep angle. Those electrodes collect ions at five vertical positions to give the ion density profile in the boundary layer, which is assumed equal to the electron number density, to be measurable between 10^{16}–10^{20} electrons/m^3. The lowest altitude where the electron density measurement can be made within this range is about 75 km. The procedure used to reduce the probe data is similar to that used with the RAM-C flight experiment.[9] Further details concerning the OREX flight measurements can be found in Refs. 2, 3, and 8.

Computational Methods

The VSL method of Ref. 1 is used to analyze flowfields over the OREX forebody for altitudes from 105 to 48.4 km (and Mach numbers from 27.1 to 9.1), whereas the DSMC method of Bird[7] is employed mostly at high altitudes (greater than about 80 km) in the present study. The VSL method can be used to compute reacting gas flows in thermochemical equilibrium or nonequilibrium state with and without body and shock-slip boundary conditions, and with an arbitrary number of chemical species.[1] For the current study, the number of species ranged from 5 to 11 using the VSL method, whereas the DSMC method used five species.

A detailed description of the VSL method that was used is given in Refs. 1 and 10. Briefly, this method is a spatial-marching, implicit, finite difference technique, which includes coupling of the global continuity and normal momentum equations. For the thermal nonequilibrium calculations with two temperatures, two energy equations are solved for the translational–rotational and vibrational–electronic–electron temperatures. Only the total energy equation needs to be solved for the thermal equilibrium calculations. Further, for the thermal nonequilibrium case, air chemistry is modeled by using a modified Arrhenius expression for the forward- and backward-rate coefficients (see Table 1 of Ref. 10). Chemical–vibrational coupling is taken into account through the preferential dissociation and recombination model proposed by Park.[11] The body and shock-slip boundary conditions are implemented at higher altitudes in the OREX trajectory. A description of the thermodynamic and transport properties, chemical kinetics model with chemical–vibrational coupling, relaxation processes for the vibrational–translational and electronic–electron–translational energies, and body and shock-slip boundary conditions is given in Refs. 1 and 10.

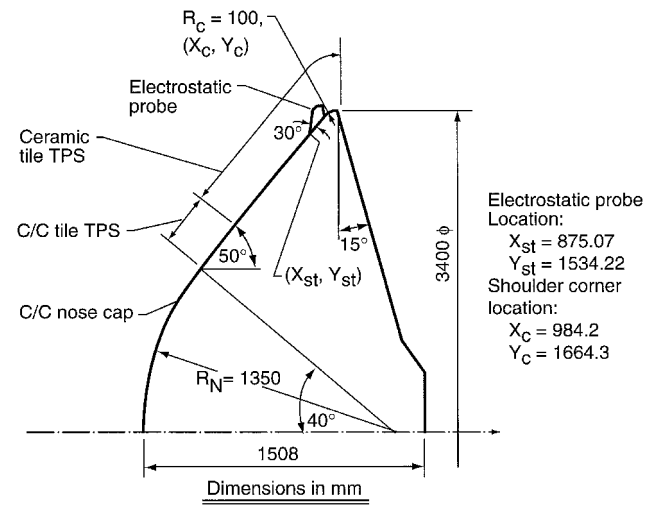

Fig. 1 Re-entry body geometry of OREX vehicle.

The surface is assumed to be noncatalytic in the present study for most of the calculations as suggested in Ref. 5. However, a finite catalytic wall boundary condition[1,12] (based on the Shuttle flight heat-flux measurements) is also implemented, which impacts the heating at altitudes lower than about 84 km. At higher altitudes, finite wall catalycity does not affect heating much as compared to a noncatalytic surface. To obtain an estimate of the reduction in heating caused by a noncatalytic (or finite catalytic) wall, some results are also obtained for a fully catalytic wall, which should be closer to the thermochemical equilibrium value.

The noncontinuum two-dimensional/axisymmetric DSMC method used herein is described in Refs. 7 and 13, and is briefly discussed here. In this method, the molecular collisions are simulated using the variable hard sphere (VHS) molecular model. The collision cross section is a function of the relative energy in the collision. Parameters used in the present study to define the VHS model are a reference temperature (2880 K), reference diameters for each of the five species (3.062×10^{-10}, 3.083×10^{-10}, 2.297×10^{-10}, 2.398×10^{-10}, and 3.065×10^{-10} m for O_2, N_2, O, N, and NO, respectively), and the temperature exponent (set to 0.73) in the power law for viscosity coefficient. Energy exchange between the kinetic and internal modes is controlled by the Larson–Borgnakke statistical model. For the diatomic molecules, a rotational relaxation collision number of 5 and a vibrational relaxation collision number of 50 are used. The gas surface interactions are modeled by assuming the gas molecules to reflect diffusively with full thermal accommodation at the specified surface temperature. Similar to the VSL calculations, the finite catalytic wall boundary condition is imposed by using the surface recombination probabilities for atomic oxygen and atomic nitrogen inferred from Shuttle data.[12]

Flight Conditions and Numerical Parameters

Table 1 provides the range of flight conditions considered, which encompass altitudes of 105–48.40 km. The atmosphere values denoted as OREX are those given in Refs. 3 and 5, where Navier–Stokes (NS) calculations were performed.

Table 1 Flight trajectory for OREX vehicle, freestream conditions

Flight time, s	Altitude, km	Velocity, m/s	T_∞, K		T_w,[a] K	Mole fractions						Specific heat ratio, γ_∞		Speed of sound, m/s		M_∞		Molecular weight, kg/k-mole		Density, kg/m^3	
						X_{O_2}		X_{N_2}		X_O											
			OREX	Jacchia		OREX	Jacchia	OREX	Jacchia	OREX	Jacchia	OREX	Jacchia	OREX	Jacchia	OREX	Jacchia	OREX	Jacchia	OREX	Jacchia
7361.0	105.00	7451.00	218	211.05	332	0.2375	0.1528	0.7625	0.7815	0.0	0.0657	1.40	1.4108	296.734	298.202	25.11	24.986	28.96	27.838	3.1400×10^{-7}	2.3350×10^{-7}
7370.6	101.10	7454.65	195	196.89	402	0.2375	0.1726	0.7625	0.7839	0.0	0.0435	1.40	1.4071	280.989	285.819	26.53	26.082	28.96	28.195	5.7100×10^{-7}	4.8341×10^{-7}
7381.0	96.77	7456.30	192	190.26	485	0.2375	0.1884	0.7625	0.7863	0.0	0.0253	1.40	1.4041	279.053	279.323	26.72	26.694	28.96	28.466	1.3810×10^{-6}	9.3644×10^{-7}
7391.0	92.82	7454.10	189	188.30	586	0.2375	0.2025	0.7625	0.7881	0.0	0.0094	1.40	1.4015	276.385	276.492	26.97	26.960	28.96	28.701	3.0090×10^{-6}	1.9465×10^{-6}
7401.0	88.45	7444.30	187	——	687	0.2375	——	0.7625	——	0.0	——	1.40	——	275.002	——	27.07	28.96	——	——	4.3060×10^{-6}	——
7411.5	84.01	7415.90	189	——	785	0.2375	——	0.7625	——	0.0	——	1.40	——	276.506	——	26.82	28.96	——	——	1.0953×10^{-5}	——
7421.5	79.90	7360.20	199	——	878	0.2375	——	0.7625	——	0.0	——	1.40	——	274.430	——	26.82	28.96	——	——	1.8455×10^{-5}	——
7431.5	75.81	7245.70	207	——	976	0.2375	——	0.7625	——	0.0	——	1.40	——	289.365	——	25.04	28.96	——	——	3.6576×10^{-5}	——
7441.5	71.73	7049.20	215	——	1091	0.2375	——	0.7625	——	0.0	——	1.40	——	295.069	——	23.89	28.96	——	——	6.5184×10^{-5}	——
7451.5	67.66	6720.30	226	——	1213	0.2375	——	0.7625	——	0.0	——	1.40	——	302.444	——	22.22	28.96	——	——	1.2164×10^{-4}	——
7461.5	63.60	6223.40	237	——	1344	0.2375	——	0.7625	——	0.0	——	1.40	——	309.776	——	20.09	28.96	——	——	2.0594×10^{-4}	——
7471.5	59.60	5561.60	248	——	1458	0.2375	——	0.7625	——	0.0	——	1.40	——	316.900	——	17.55	28.96	——	——	3.3131×10^{-4}	——
7481.5	55.74	4759.10	259	——	1531	0.2375	——	0.7625	——	0.0	——	1.40	——	323.528	——	14.71	28.96	——	——	5.3150×10^{-4}	——
7491.5	51.99	3873.40	268	——	1557	0.2375	——	0.7625	——	0.0	——	1.40	——	328.254	——	11.80	28.96	——	——	8.2445×10^{-4}	——
7501.5	48.40	3000.00	271	——	1388	0.2375	——	0.7625	——	0.0	——	1.40	——	331.126	——	9.06	28.96	——	——	1.2677×10^{-3}	——

[a]CFD inferred stagnation surface temperatures of Yamamoto.[5] Also, temperature distributions are specified from the same CFD computations.

These values are similar to those for the 1962 U.S. Standard Atmosphere[14] up to an altitude of about 90 km. For altitudes above 90 km, the atmospheric properties given by Jacchia[15] (for an exospheric temperature of 1200 K) are employed. Jacchia values[15] have been used extensively in previous high-altitude studies.[16,17] These values differ from those given by the OREX atmosphere[3] and avoid a significant change in the slope of the density-vs-altitude curve around 90 km altitude (see Fig. 2 of Ref. 18). The density values from the Jacchia atmosphere[15] are lower by about one-third from those given by Yamamoto and Yoshioka[3] (Table 1) at higher altitudes.

The stagnation-point temperatures (Table 1) and surface temperature distributions (see Fig. 3a of Ref. 18) employed in the present study are those obtained by Yamamoto[5] for altitudes of 105 km, and below 105 km, using a Navier–Stokes solution for the flowfield coupled with a material response code as described in Ref. 3. The considerable temperature variations shown in Fig. 3a of Ref. 18 as a function of distance along the surface are caused by variations in materials, material thicknesses, and material thermal properties. The carbon–carbon nose cap with a thickness of 0.4 mm extends to a wetted length of $s = 0.942$ m (measured from the stagnation point). Following the nose cap are the carbon–carbon tiles that terminate at $s = 1.242$ m and then four rings of silica tiles, having much lower conductivities and, hence, higher surface temperatures, extend to $s = 1.982$ m. The corner shoulder is also protected with a fifth ring of silica tiles. The computations of Ref. 5 for the backside surface temperature are different from those of Ref. 3 for two reasons:

1) Thermal properties of the C/C nose cap are changed to new values.

2) Internal emission from the C/C nose is assumed to be zero by the heat shield effects, as recommended by the industry.

These two changes result in a C/C nose cap temperature history, calculated by the coupled Navier–Stokes/material response [CFD–FEM (finite element method)] code, to agree better with the flight temperature history for the altitude range of 105–45 km.

The VSL calculations have been done by using a normal grid with 101 points, which are clustered both at the body surface and shock to capture large gradients in the flow properties at these locations for the low-density flows. The points are clustered only at the body surface at higher densities. The grid spacing is varied from 1×10^{-6} to 1×10^{-4} m to obtain a grid-independent solution for the altitude range given in Table 1. The smallest grid is used at the lowest altitude of 48.40 km and is increased in inverse proportion to the density for higher altitudes. In the streamwise direction, a minimum grid spacing of 2×10^{-2} m is used.

For the DSMC calculations,[13] the size of computational cells adjacent to the body surface in the direction normal to the surface is usually less than half of the local mean free path length, and for most solutions they are much smaller. Previous experience[16] has shown that such a resolution adjacent to a surface provides results that are independent of further cell refinement. For the lower altitude cases, the computational cells had very large aspect ratios with the dimensions along the surface equal to many local mean free path lengths.

The NS results of Refs. 3 and 5 were obtained with the thin-layer NS equations coupled with a FEM solver that models the heat transfer within the thermal protection material and provides the wall temperature boundary condition for the NS solver. The FEM solver accounted for both temperature and directional property dependence of the thermal protection materials considered.[3] An outline of the coupling procedure between the NS and FEM solvers is given in Ref. 3. The NS results employed the following modeling features: no-slip and noncatalytic surface boundary conditions, and a 1-T, seven-species nonequilibrium chemistry model. The unpublished results of Ref. 5 (used in the present work for comparison) were

obtained recently and differ from those reported in Ref. 3, in that the agreement between the computed and flight-measured back surface temperature was improved for the reasons mentioned earlier.

The inferred flight data shown with the results presented here are taken from Ref. 3 and are referred to as inferred from flight. The procedures used to obtain these data are described in Ref. 8.

Results and Discussion

Results are presented from the detailed VSL calculations for flowfield and surface quantities at altitudes of 92.82, 88.45, 84.01, and 59.60 km (peak-heating altitude in Ref. 3). These results are compared with other calculations and also with the OREX flight data for electron density and stagnation-point heating.

Calculation for Flowfield and Surface Quantities

Before comparing the present results with other calculations and flight data, it is useful to have an indication of the sensitivity of the VSL calculations to various parameters that are employed to define the problem. Some of the parameters considered are the number of species in the chemistry model, surface catalytic activity, and freestream density. A variation in the values of these parameters gives an indication of the sensitivity of computed results to the uncertainty in their specified values. Main results of the sensitivity study[18] are presented and briefly discussed first. Next, an assessment of thermochemical nonequilibrium and slip effects is provided. A comparison of the VSL calculations with DSMC and NS predictions is included at the end of this section.

Sensitivity to Number of Species in a Chemistry Model

The stagnation heating for a noncatalytic surface for two-temperature (2-T), 5-species (O, O_2, N, N_2, and NO), 7-species (O, O_2, N, N_2, NO, NO^+, and e^-), and 11-species (O, O_2, N, N_2, NO, O^+, O_2^+, N^+, N_2^+, NO^+, and e^-) chemistry models is given in Ref. 18. Effect on stagnation heating is shown to be negligible when the number of species is increased from 7 to 11 (Ref. 18). Therefore, a seven-species chemistry model is considered adequate for the present study.

Sensitivity to Surface Catalytic Activity

The surface heating calculations are made with the assumptions of noncatalytic, finite catalytic, and fully catalytic walls. The finite catalytic surface recombination values employed are those of Ref. 12. For the 84.01 km altitude results shown in Fig. 2a, the surface temperatures are less than about 1100 K and the recombination probabilities for the finite catalytic wall in this figure are less than 3.25×10^{-3} and 9.35×10^{-4} for atomic oxygen and nitrogen, respectively. With these low values of the recombination probabilities, the calculated heat transfer rates are essentially the same as those for the noncatalytic wall case. However, at 59.60 km altitude (see Fig. 2b), the maximum recombination probability values for atomic oxygen and nitrogen increase to 2.20×10^{-2} and 1.50×10^{-3}, respectively, at the stagnation point where the temperature is about 1460 K. For a noncatalytic wall, a 34% reduction in VSL stagnation heating prediction is obtained for this case and for a fully catalytic wall, this heating rate is increased by about 31%. For a 84.01 km altitude (Fig. 2a), the VSL heating rate for the fully catalytic wall condition is substantially larger, as compared to the noncatalytic (or finite catalytic) wall values. The VSL calculations at a 84.01 km altitude (Fig. 2a) employ a 2-T formulation with the surface and shock-slip boundary condition, whereas a 1-T model with a no-slip boundary condition is used at the altitude of 59.60 km (Fig. 2b) to reflect appropriate flowfield physics in the computations.

Figures 2a and 2b also contain the 1-T NS calculations of Yamamoto[5] for a noncatalytic wall with zero surface slip. Also

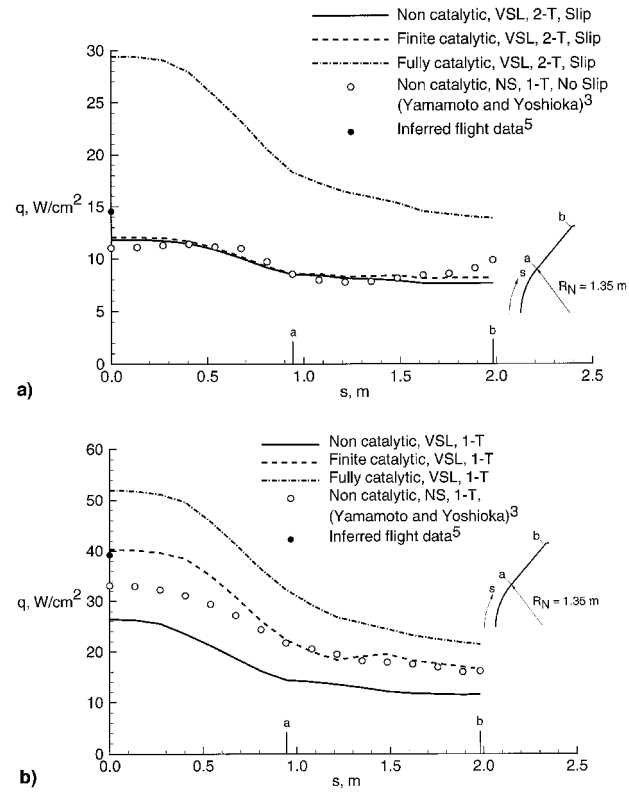

Fig. 2 Effect of surface catalytic activity on surface heating rate: a) altitude = 84.01 km ($Kn_\infty = 0.0016$) and b) altitude = 59.60 km ($Kn_\infty = 7.35 \times 10^{-5}$).

shown in Fig. 2 are the OREX stagnation inferred flight data for comparison. Present VSL calculations for a finite catalytic wall are in good agreement with reported flight data for the altitude of 59.60 km (Fig. 2b). At 84.01 km altitude (Fig. 2a), however, these calculations are lower by about 17% as compared to the data. Assuming the surface to be noncatalytic at lower altitudes will result in lower heating as compared to the inferred flight data as seen from Fig. 2b. The NS calculations of Ref. 5 also give surface heating distributions, which compare well at the altitude of 84.01 km (e.g., Fig. 2a). However, the results of Ref. 5 appear at variance at the altitude of 59.60 km with the catalytic boundary condition employed in the present calculations.

Sensitivity to Freestream Density

Actual atmospheric density during re-entry can be a significant uncertainty for a given altitude/time, particularly at the higher altitudes. It may differ significantly from that obtained from a standard atmospheric model.[14,15] The significance of this effect on surface heating is shown in the Comparison with Flight Data section later in this paper.

Assessment of Thermochemical Nonequilibrium and Slip Effects

An evaluation of thermochemical nonequilibrium in the flowfield can be made by analyzing the temperature profiles and surface distributions of pressure and heating rate for a noncatalytic wall. The stagnation profiles for the translational–rotational T and T_{ve} temperature ratios are shown to be quite different for the altitude of 92.82 km through the entire shock layer, and accordingly, thermal nonequilibrium extends all the way to the surface.[18] The degree of nonequilibrium in the two temperature profiles, however, is shown to be reduced closer to the surface at 84.01 km altitude.[18]

Effects of thermal nonequilibrium on surface quantities may be evaluated by analyzing the pressure distributions given in Figs. 3a and 3b from the continuum (VSL) and DSMC methods.

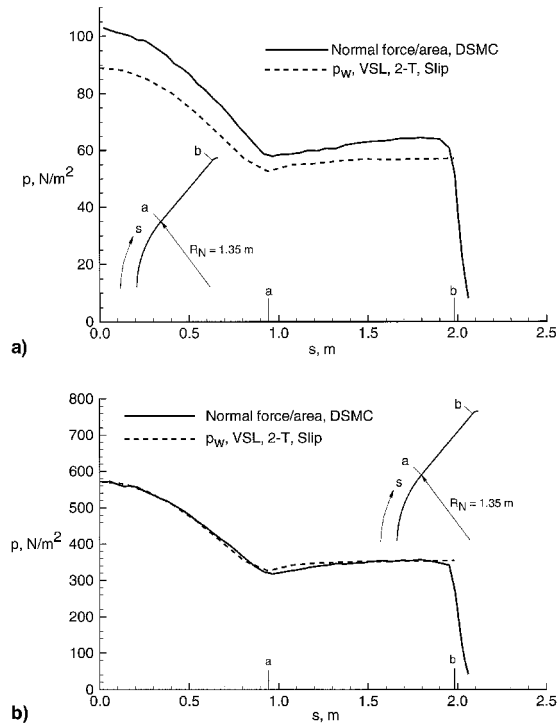

Fig. 3 Surface pressure distribution: a) altitude = 92.82 km (Kn_∞ = 0.0086) and b) altitude = 84.01 km (Kn_∞ = 0.0016).

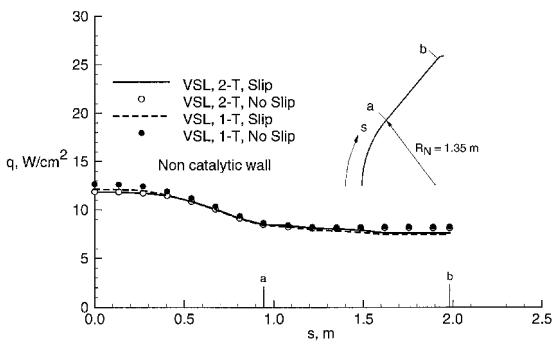

Fig. 4 Surface heating-rate distribution (altitude = 84.01 km).

Unlike the continuum calculations, where assumptions are made with regard to the pressure tensor, a DSMC calculation accounts for nonisotropic effects that become significant under rarefied (thermal nonequilibrium) conditions. Therefore, normal force per unit area is shown in these figures from the DSMC calculations for comparison with the p_w distribution obtained from the VSL computations. Under thermal equilibrium conditions, the isotropic pressure p_w and normal force per unit area are the same.[7] The surface distributions of these two quantities are different at the altitude of 92.82 km (Fig. 3a), suggesting the influence of thermal nonequilibrium on p_w, which is increased by about 20%. At 84.01 km altitude (Fig. 3b), however, distributions of normal force/area and p_w essentially have the same values, which imply conditions close to thermal equilibrium.

To assess the effect of thermal nonequilibrium on surface heating rate at a 84.01 km altitude, heating-rate distributions are computed (Fig. 4) using 1-T (for thermal equilibrium) and 2-T (for thermal nonequilibrium) models with the VSL method. Also, results are obtained with and without shock and surface-slip conditions. The VSL results of Fig. 4 imply that the effects of both thermal nonequilibrium and slip are insignificant on surface-calculated quantities for the 84.01 km altitude conditions, and these effects may be neglected in calculations below this altitude.

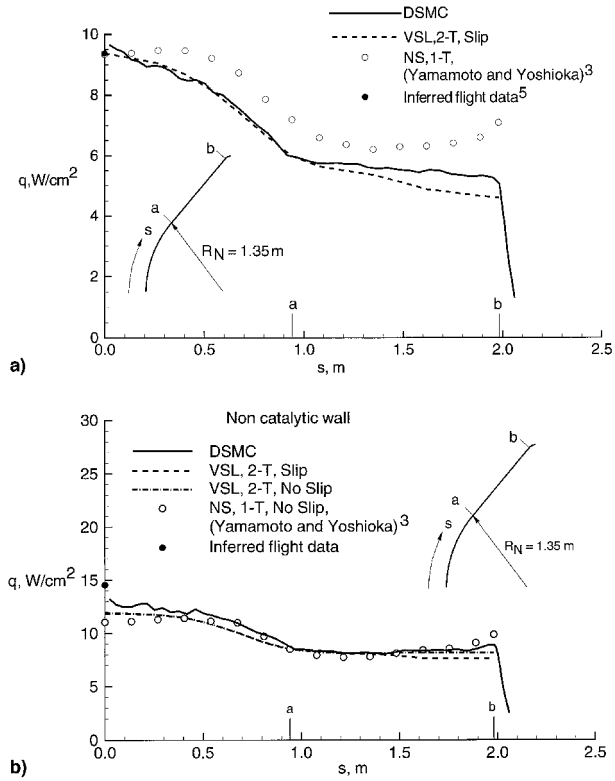

Fig. 5 Comparison of surface heating-rate distribution: a) altitude = 92.82 km (Kn_∞ = 0.0086) and b) altitude = 84.01 km (Kn_∞ = 0.0016).

Comparison with Direct Simulation Monte Carlo (DSMC) and NS Calculations

Surface heating-rate distributions obtained using the VSL method are compared with those obtained from DSMC and NS calculations in Figs. 5a and 5b, at altitudes of 92.82 and 84.01 km, respectively. Also shown are the flight-inferred data for the stagnation-point heating. Except for the results shown over the conical flank in Fig. 5a, there is generally a good agreement between the VSL and DSMC calculations for the two altitudes (Figs. 5a and 5b). This implies that a 2-T VSL formulation with slip boundary conditions models the low-density effects (thermal nonequilibrium and slip) quite well. The NS calculations of Ref. 5 are also in good agreement with the present results in the stagnation region at 92.82 km altitude (Fig. 5a), and along most parts of the OREX forebody at 84.01 km altitude (Fig. 5b). It is not obvious, however, why the NS results of Ref. 5 away from the stagnation region are higher in Fig. 5a. Generally, the influence of a shoulder expansion on the upstream surface heating should become negligible at higher altitudes. The surface heating becomes a function of only surface inclination at free molecular flow conditions. Present calculations agree quite well with the stagnation flight data at 92.82 km altitude. However, the present results are lower than the flight data by about 17% at 84.01 km altitude. Also, some slip effects are noticeable over the conical flank at this altitude (Fig. 5b).

Additional comparisons of the present results with DSMC and NS calculations and flight data at the stagnation point are provided in the next section.

Comparison with Flight Data

This section provides a comparison between the computed and flight-inferred stagnation-point heating rates along the trajectory and electron number densities (measured from the electrostatic probe mounted near the shoulder of the vehicle).

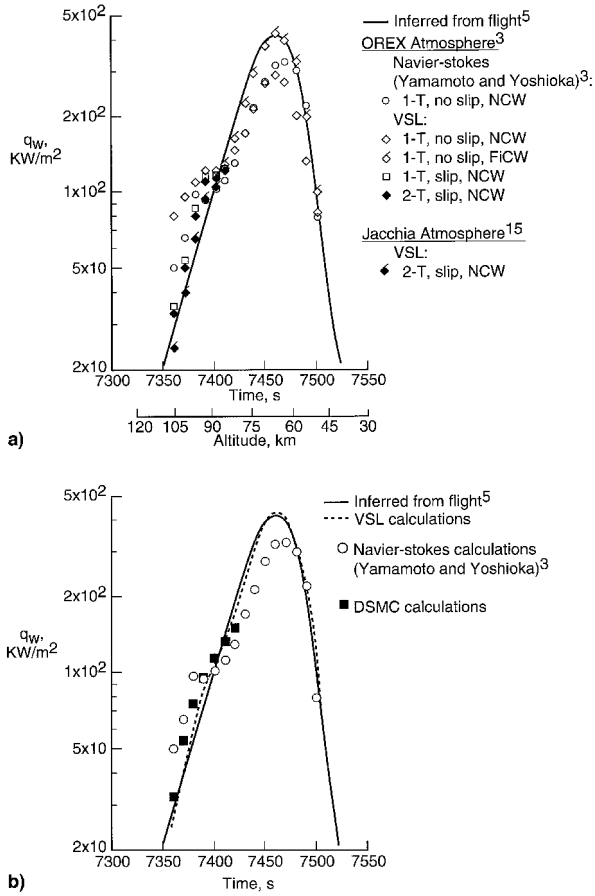

Fig. 6 Comparison of predicted stagnation-point heat transfer rates with inferred flight data: a) VSL and NS calculations and flight data and b) VSL, NS, and DSMC calculations and flight data.

Stagnation-Point Heating

Figures 6a and 6b present VSL results (for altitudes of 105–48.4 km) as a function of flight time from launch. The DSMC calculations for altitudes of 105–79.9 km are shown in Fig. 6b. Also shown in Figs. 6a and 6b are the NS calculations (called CFD–FEM results in Ref. 3) of Yamamoto.[5]

Since atmospheric data was not gathered during the OREX flight experiment, calculations of Refs. 3 and 5 are based on the atmospheric conditions given in Ref. 3, which is referred to as OREX atmosphere in Fig. 6a and Table 1. Also shown in Fig. 6a are the VSL calculations based on the Jacchia atmosphere model[15] for altitudes above 90 km (see Table 1 for the two models). As can be seen from Fig. 6a, the 2-T VSL predictions for a noncatalytic wall (with slip) based on the Jacchia atmosphere[15] are in better agreement with inferred flight data between the 90–105 km altitude range as compared to both the NS and VSL calculations utilizing the OREX atmospheric data. Further, the effect of slip on surface heating is dominant, whereas the thermal nonequilibrium (2-T) effects are secondary in this altitude range. Both slip and thermal nonequilibrium (2-T) effects are neglected in the NS calculations.[3,5]

For altitudes below 84.01 km, surface temperatures are higher and slip and thermal nonequilibrium effects become negligible. At higher temperatures, finite surface catalytic activity also begins to influence the heating rate. Therefore, a 1-T, no-slip, and finite catalytic wall flow model is appropriate for the lower altitude calculations. The VSL calculations with these flow assumptions are in better agreement with the inferred flight data than the 1-T, no-slip, noncatalytic VSL and NS calculations (Fig. 6a).

Figure 6b shows a comparison between VSL, NS, and DSMC predictions, and with the inferred flight data. The dotted line in Fig. 6b is a fairing through the VSL-predicted values with appropriate flow physics from high-to-low flight altitudes. The DSMC results are shown for the high-altitude range of 105–79.9 km. Overall, the qualitative behavior of the DSMC results is similar to that of VSL calculations, and there is a good agreement between the two and with the inferred flight data. The NS [1-T, no slip, noncatalytic wall (NCW)] calculations of Yamamoto[5] are higher for altitudes greater than 88.45 km as compared to the VSL and DSMC calculations as well as the inferred flight data. As explained earlier, noninclusion of thermal nonequilibrium and slip effects at higher altitudes and nonimplementation of the finite catalytic wall boundary condition at lower altitudes with the NS computations[3,5] may be responsible for the differences with the VSL and DSMC predictions.

As described in the Introduction section, the OREX vehicle was enclosed in a protective fairing during launch, thereby negating the requirement for waterproofing the thermal protection materials. Since the Shuttle Orbiter is an operational vehicle, waterproofing procedures are employed. Therefore, the OREX thermal protection system should not produce some of the outgassing products and consequent reduction in heating that is evident for the Orbiter[4] during the initial portion of the heat pulse. The surface heat transfer coefficient based on the initial entry heating data reported for OREX exhibits[13] a monotonic increase with the increase in Knudsen number. This type of behavior is characteristic of the hypersonic cold-wall, stagnation-point heating for a nonblowing surface.[19,20]

Electron Number Density

Flight data for the electron number density distribution in the boundary layer with strong entropy layer swallowing serve to delineate the applicability of 2-T and 1-T flow models for nonequilibrium ionized gas flows. An accurate calculation of the electron density also provides knowledge of the onset and expiration of the communication blackout phase during entry.

Figure 7 shows the electron number density time history at the location of probe 5 (see Fig. 1c of Ref. 18). Two sets of data shown in Fig. 7 are reduced,[2,5] by using 1-T and 2-T CFD methods of Ref. 6, which employs NS equations with a seven-species chemical model, and Park's[11] two-temperature model for the 2-T calculations. Also shown in Fig. 7 are predictions reported in Ref. 2. The signal conditioner of the electrostatic probe is adjusted to measure the electron density in the 10^{16} – 10^{20} particles/m^3 range.

Present VSL calculations are given at the three altitudes of 92.82, 88.45, and 84.01 km or the flight times of 7391, 7401, and 7411.5, respectively, in Fig. 7. These calculations were performed with 1-T and 2-T flow models and slip boundary

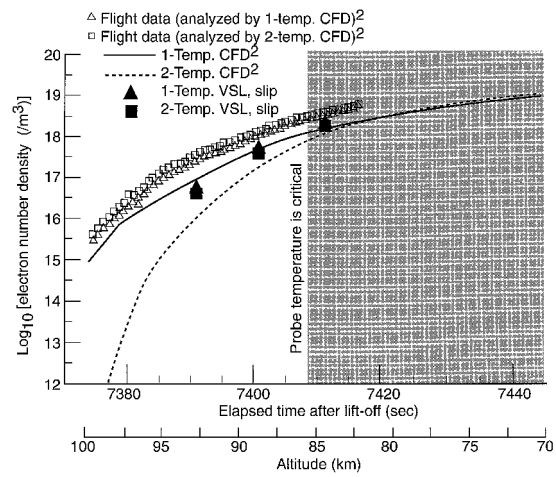

Fig. 7 Electron number density history for probe 5 (s = 1.9135 m, n = 5.8335 × 10^{-2} m).

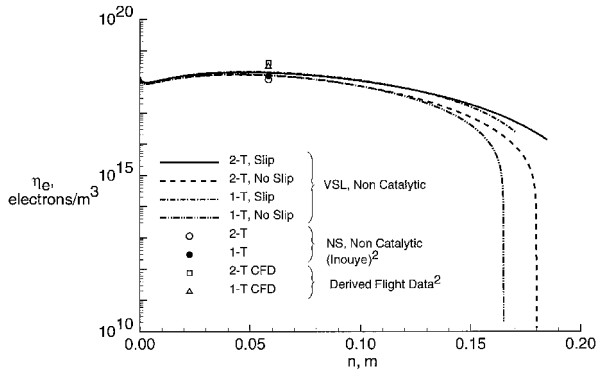

Fig. 8 Electron number density profiles at probe 5 location (s = 1.9135 m, n = 5.8335 × 10^{-2} m) for altitude = 84.01 km (Kn_∞ = 0.0016).

conditions. Present 1-T VSL predictions are slightly higher than the 2-T VSL results. Both of these VSL calculations are closer to the data and 1-T CFD calculations than are the 2-T CFD results for all three probe locations shown in Fig. 7. Similar to the surface heating results given earlier, the effect of thermal nonequilibrium on electron density also appears to be secondary. The observation of Ref. 2, that the flight data agree better with 1-T flow model, is not necessarily the case for the present calculations. For flight times earlier than 7401 s, i.e., at higher altitudes, when the low-density effects (such as thermal nonequilibrium and slip) become important, a 2-T flow model with slip should be more realistic as evidenced by the good agreement between the 2-T VSL and DSMC calculations shown earlier.

Finally, Fig. 8 shows further detailed comparisons between the predicted values and data for the electron density profiles at the altitude of 84.01 km for the location of probe 5. The VSL predictions in Fig. 8 have been obtained with the assumptions of thermal nonequilibrium (2-T) and equilibrium (1-T) with and without the slip boundary conditions. Except for the narrow region near the shock, the electron density profiles (similar to the surface heat transfer rates) are predicted essentially by the thermal-equilibrium, no-slip flow model. The electron density profiles pass almost through the flight-measured value (Fig. 8). Also, present VSL predictions are in good agreement with the NS results at this altitude.[2]

Summary and Conclusions

This study presents a VSL analysis of the re-entry flowfield around the forebody of the OREX vehicle. The OREX vehicle is a 50-deg, half-angle spherically blunted cone with a nose radius of 1.35 m and a base diameter of 3.4 m. Calculations are performed for an altitude range of 105–48.4 km. In this altitude range, the flowfield character changes from thermal nonequilibrium to thermal equilibrium, and the slip effects become insignificant at lower altitudes. The low-density effects (such as thermal nonequilibrium and slip) at higher altitudes are accounted for in the VSL method through the 2-T formulation with slip boundary conditions. With the disappearance of these effects at lower altitudes, VSL results are computed using a 1-T flow model with no-slip boundary conditions. Present results are compared with the flight data and existing NS calculations for the OREX trajectory, and with DSMC results at higher altitudes in this trajectory.

Results from calculations with 5-, 7-, and 11-species air models reveal that the 7-species chemical model is adequate to analyze the OREX flowfield. Inclusion of low-density effects (i.e., both thermal nonequilibrium and slip) is important for altitudes greater than 84 km. This is demonstrated by the comparison of viscous shock-layer results obtained from one-temperature, no-slip, and two-temperature, slip-flow models. Surface catalytic activity also significantly influences the level of heating at altitudes lower than 84 km in the trajectory. At the peak heating altitude of 59.60 km, a 50% reduction in stagnation-region heating is obtained for a noncatalytic wall as compared to a fully catalytic wall. Reduction in heating is about 23% for a finite catalytic surface with recombination probabilities similar to those of the Shuttle Orbiter thermal protection coatings. However, at higher altitudes, the recombination probabilities are quite low and the calculated heating for altitudes greater than about 84 km is essentially the same as that for a noncatalytic surface.

In general, there is a good agreement between the VSL predictions and the OREX measured or inferred data for electron number density and stagnation-point heat transfer rate. Present results compare quite well with the DSMC predictions for altitudes higher than about 84 km. The earlier NS calculations are higher at high altitudes because of the noninclusion of low-density effects, and the calculations are lower at low altitudes because of use of noncatalytic wall boundary conditions when compared with the flight-inferred heat transfer rate data.

The OREX heat transfer rate data may be unique for high-altitude flight conditions in that they exhibit proper qualitative behavior with increasing altitudes. With further refinements in data extraction procedures and definitions, a valuable aerothermodynamic database will become available. This database should prove immensely helpful in validating the use of various theoretical models used for simulation and provide a test of flowfield codes for reacting gas flows.

References

[1]Gupta, R. N., "Viscous Shock-Layer Study of Thermochemical Nonequilibrium," *Journal of Thermophysics and Heat Transfer*, Vol. 10, No. 2, 1996, pp. 257–266.

[2]Inouye, Y., "OREX Flight-Quick Report and Lessons Learned," *2nd European Symposium on Aerothermodynamics for Space Vehicles*, European Space Agency, SP-367, Paris, France, 1995, pp. 271–279.

[3]Yamamoto, Y., and Yoshioka, M., "CFD and FEM Coupling Analysis of OREX Aerothermodynamic Flight Data," AIAA Paper 95-2087, June 1995.

[4]Moss, J. N., and Bird, G. A., "Direct Simulation Transitional Flow for Hypersonic Re-Entry Conditions," *Thermal Design of Aeroassisted Orbital Vehicles*, edited by H. F. Nelson, Vol. 96, Progress in Astronautics and Aeronautics, AIAA, New York, 1985, pp. 113–139.

[5]Yamamoto, Y., "Tabulated Values for Temperature and Heat Transfer Distributions," Aerodynamics Div., National Aerospace Lab., Tokyo, Japan, Dec. 1995.

[6]Watanabe, Y., Inouye, Y., Wada Y., Akimoto, T., and Fujiwara, T., "Computational and Experimental Studies on an Electrostatic Probe and Catalytic Effect Sensor for a Reentry Experiment," AIAA Paper 93-0479, Jan. 1993.

[7]Bird, G. A., *Molecular Gas Dynamics and the Direct Simulation of Gas Flows*, Clarendon, Oxford, England, UK, 1994.

[8]"Orbital Re-Entry Experiment," NAL/NASDA Joint Research Report, March 1995 (in Japanese).

[9]Jones, W. L., Jr., and Cross, A. E., "Electrostatic Probe Measurements of Plasma Parameters for Two Reentry Flight Experiments at 25000 Feet Per Second," NASA TN D-6617, April 1972.

[10]Gupta, R. N., "Viscous Shock-Layer Study of Thermochemical Nonequilibrium," AIAA Paper 95-2083, June 1995.

[11]Park, C., *Nonequilibrium Aerothermodynamics*, Wiley, New York, 1990, pp. 103–115.

[12]Gupta, R. N., "Reevaluation of Flight-Derived Surface Recombination-Rate Expressions for Oxygen and Nitrogen," *Journal of Spacecraft and Rockets*, Vol. 33, No. 3, 1996, pp. 451–457.

[13]Moss, J. N., Gupta, R. N., and Price, J. M., "DSMC Simulations of OREX Entry Conditions," 20th International Symposium on Rarefied Gas Dynamics, Beijing, PRC, Aug. 1996.

[14]Anon., *U.S. Standard Atmosphere*, U.S. Government Printing Office, Washington, DC, Dec. 1962.

[15]Jacchia, L. C., "Thermospheric Temperature, Density and Composition: New Modes," *Research in Space Science*, Smithsonian Inst. Astrophysical Observatory, Special Rept. 375, Cambridge, MA, March 1977.

[16]Celenligil, M. C., Moss, J. N., and Blanchard, R. C., "Three-Dimensional Rarefied Flow Simulations for the Aeroassist Flight Experiment Vehicle," *AIAA Journal*, Vol. 29, No. 1, 1991, pp. 52–57.

[17]Gupta, R. N., "Stagnation Flowfield Analysis for an Aeroassisted Vehicle," *Journal of Spacecraft and Rockets*, Vol. 30, No. 1, 1993, pp. 14–21.

[18]Gupta, R. N., Moss, J. N., and Price, J. M., "Assessment of Thermochemical Nonequilibrium and Slip Effects for Orbital Reentry Experiment (OREX)," AIAA Paper 96-1859, June 1996.

[19]Gupta, R. N., and Simmonds, A. L., "Hypersonic Low-Density Solutions of the Navier-Stokes Equations with Chemical Nonequilibrium and Multicomponent Surface Slip," AIAA Paper 86-1349, June 1986.

[20]Moss, J. N., Cuda, V., Jr., and Simmonds, A. L., "Nonequilibrium Effects for Hypersonic Transitional Flows," AIAA Paper 87-0404, Jan. 1987.